An Ab Initio Analysis of Structural and Electronic Properties of Cubic SrSnO₃

Marta Maria de Moura Bezerra [iD] [a], Marisa Carvalho Oliveira* [iD] [b], Weber Duarte Mesquita [iD] [a], Amilton Brito da Silva Junior [c], Elson Longo [iD] [b], and Maria Fernanda do Carmo Gurgel [iD] [a,d]

This article reports a theoretical study on structural and electronic properties of the cubic strontium stannate (SrSnO₃) using periodic quantum-mechanics calculations within the Density Functional Theory method combined with B3LYP exchange-correlation functional, as implemented in the CRYSTAL14 code. The results were analyzed using the energy level diagram, atomic orbital distributions, and electron density maps. The structural analysis confirmed the SrSnO₃ cubic symmetry, and the electronic properties were associated with [SrO₁₂] and [SnO₆] clusters with distinct bonding character. Furthermore, our structural and electronic calculations are in good agreement with the available experimental data showing a mean percentage error close to 2.2% for the structural parameter and paving the avenue towards the complete understanding of the overall properties of perovskite materials.

Graphical abstract
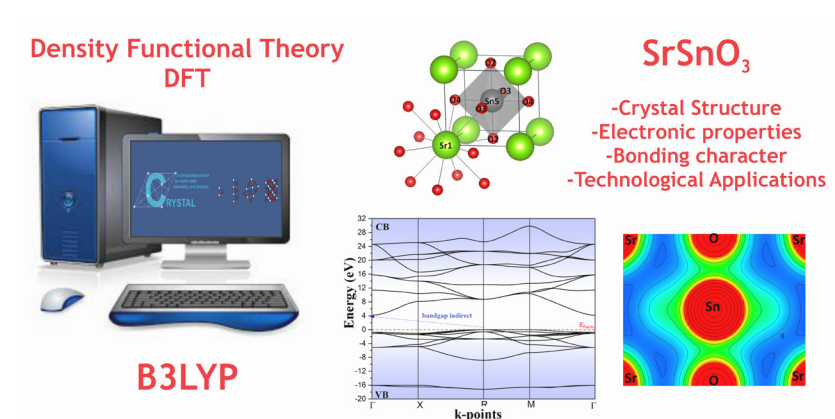
1. Introduction

Tin-based perovskite oxides have the general formula ASnO₃. One of the main compounds of this class of materials is the alkaline earth stannates perovskites, for which site A is occupied by calcium (Ca), strontium (Sr), or barium (Ba) with an ionic radius ranging from 100 pm, 118 pm and 135 pm, respectively [1, 2]. Alkaline earth stannates have been used mainly to produce transparent electrodes for various applications, particularly in photovoltaic cells and light-emitting organic diodes. ASnO₃ are also widely used in the electronics industries due to their superior dielectric and gas-sensing properties. Furthermore, they are promising materials for photocatalytic degradation and hydrogen production [2-8].

[a] Institute of Physics, PPGCET, Federal University of Catalão, Av. Dr. Lamartine Pinto de Avelar, Catalão - GO, 75704-020, Brazil. [b] Functional Materials Development Center, Federal University of São Carlos, São Carlos - SP, 13565-905, Brazil. [c] Department of Mining Engineering, Federal University of Catalão, Av. Dr. Lamartine Pinto de Avelar, Catalão - GO, 75704-020, Brazil. [d] Institute of Chemistry, Federal University of Catalão, Av. Dr. Lamartine Pinto de Avelar, Catalão - GO, 75704-020, Brazil. *Corresponding author. E-mail: **marisacoliveira31@gmail.com**

Special attention is given to strontium stannate structure ($SrSnO_3$), the focus of this manuscript. The crystalline structure of $SrSnO_3$ is formed from Sr^{2+} ions surrounded by 12 oxygen atoms occupying a dodecahedral site originated by four [SnO_6] octahedrons. These octahedrons are formed by oxygen that occupies the vertices, and the Sn^{4+} cation is located in the center of the structure. The unit cell of $SrSnO_3$ corresponds to a distorted cube due to the octahedral inclination that generates an orthorhombic structure (space group *Pbnm*) at room temperature [9, 10]. However, $SrSnO_3$ can exist as other polymorphs (*Imma*, *I4/mcm*, and *Pm$\overline{3}$m*) depending upon the temperature increase due to very high mobility and concentration of carriers [10-13].

In particular, due to the scientific and technological interest in its applications, $SrSnO_3$, in the form of powder or films, is obtained by different synthesis methods. Gao et al. [14] showed the obtaining of $SrSnO_3$ through the conventional solid-state reaction at high temperatures, combining an experimental investigation associated with a theoretical approach through DFT calculations using the LDA method, as implemented in the CASTEP code to elucidate the effects of epitaxial tension on thin $SrSnO_3$ films. Similarly, a study developed by Zhang et al. [10] used DFT calculations implemented in the VASP simulation package and the revised Perdew-Burke-Ernzerhof function for solids (PBEsol) for structural relaxation and Heyde-Scuseriae-Ernzerhof (HSE06) for the electronic structure analysis in order to elucidate the ferroelectricity induced by $SrSnO_3$ deformation and coupling, showing promising photovoltaic properties for application in solar cell devices.

In this paper, the novelty is highlighted with current progress on first-principles calculations performed for $SrSnO_3$ based perovskite compounds to demonstrate that the electronic properties are associated with the presence of different clusters with a unique bonding environment from electron density distribution. Moreover, the structural properties were analyzed in detail, establishing a structure-property relationship to explain the electronic structure and the bandgap (E_{gap}) region.

2. Results and Discussion

The optimized bulk structure of the cubic $SrSnO_3$ perovskite (*Pm$\overline{3}$m*) exhibit lattice parameters a = b = c = 4.08 Å, angles α = β = γ = 90°. The fractional coordinates were obtained as (0.0.0) for the Sr atom, (0.5, 0.5, 0.5) for the Sn atom, while the O atoms were described by (0.5, 0.5, 0); (0, 0.5, 0.5) and (0.5, 0, 0.5), resulting in a model containing 5 atoms (see Figure 1).
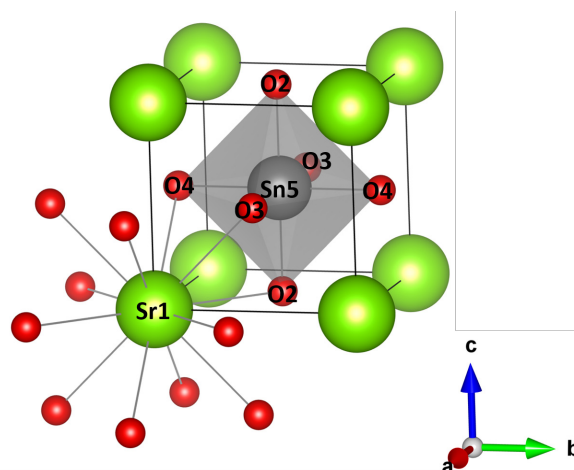
Fig. 1. The enumerated unit cell for cubic perovskite $SrSnO_3$.

The structural results reported in this work compared to other experimental and theoretical values available in the literature are shown in Table 1.

Table 1. Lattice parameters (Å), unit cell volume (Å³), and bond distances between M-O (M = Sr and Sn) atoms of the $SrSnO_3$ cubic bulk.

Perovskite SrSnO₃	Lattice parameters a=b=c	Unit cell volume	Bond Distances		Reference
			Sr-O	Sn-O	
This Work	4.080	67.917	2.885	2.040	--
Experimental	4.025	65.226	2.846	2.012	[15]
Experimental	4.034	65.645	-	-	[16, 17]
Experimental	4.027	65.304	-	-	[18]
Experimental	4.032	65.548	-	-	[19, 20]
Experimental	4.040	65.939	-	-	[21]
Theoretical	4.111	69.477	-	-	[22]

The values of the lattice parameters and the MO bond distances (M = Sr and Sn) obtained in the present study agree with the values obtained experimentally regarding the data of ICSD nº 27047 [15]. Besides, we estimate a lower percentage error (1.366 %) for the obtained lattice parameters. In comparison, the percentage error for the bond distances was obtained as 1.370 % for Sr-O and 1.391% for Sn-O. On the other hand, the theoretical values found in the literature (Table 1) presented a percentage error greater than 2.136 % for the cubic lattice parameters compared to the experimental data, thus indicating that our computational model presents better proximity to the experimental works.

From the optimized structure of the bulk $SrSnO_3$ (Table 1), it was possible to build a simulated X-ray diffractogram (XRD) using the VESTA program, as depicted in Figure 2. It was possible to note the respective peaks corresponding to the single cubic phase in red lines consistent with the experimental results of $SrSnO_3$ obtained using the polymeric precursor method and thermally treated at a temperature of 1000 °C, as reported by Cassia-Santos *et al*. [18]

Understanding the materials electronic structure is also a fundamental point in the discovery of new materials with unique or desirable properties. Thus, at first, the electronic properties were analyzed by band structure and density of state (DOS) projected on the atoms and atomic orbitals of Strontium, Tin, and Oxygen, as shown in Figure 3(a-d).

The integration of the reciprocal space for all calculations of $SrSnO_3$ material followed the k-points Γ (0,0,0) - X (½, 0,0) -

R (½, ½, ½) - M (½ , ½, 0) - Γ (0,0,0), as shown in Figure 3a. In Figure 3b, it was observed that the bandgap for $SrSnO_3$ is an indirect transition between the k-points R-Γ with a value equals to 4.18 eV. Analyzing the DOS projection (Figure 3c), it was noted that the valence band (VB) region is observed between -17.91 and 0 eV, while the conduction band (CB) region is located between 4.18 and 29.84 eV. Figure 3d shows the DOS projection for the atomic orbitals of Sr, Sn, and O atoms, showing that the three oxygen atoms have equivalent contributions and present the major contribution along with the VB through the 2s and 2p (x, y, z) orbitals combined with a minor extent of the Sr atomic orbitals 4p (x, y, z). On the other hand, the Sn atoms contribute more significantly in CB with the 5s, 5p (x, y, z), and 5d (xz, yz and xy) orbitals.
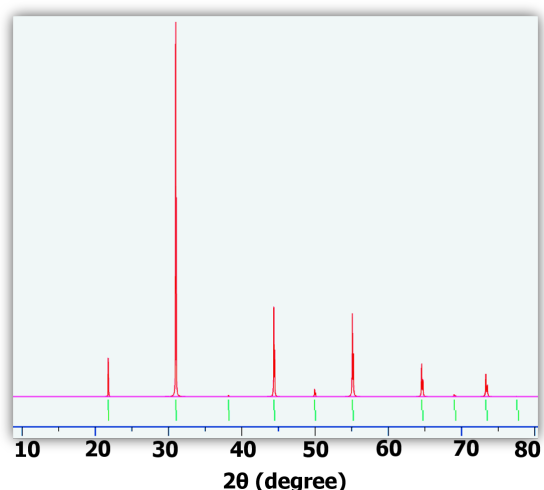
Fig. 2. Simulated X-Ray diffractogram of the $SrSnO_3$. The simulated XRD patterns were obtained using the VESTA program.
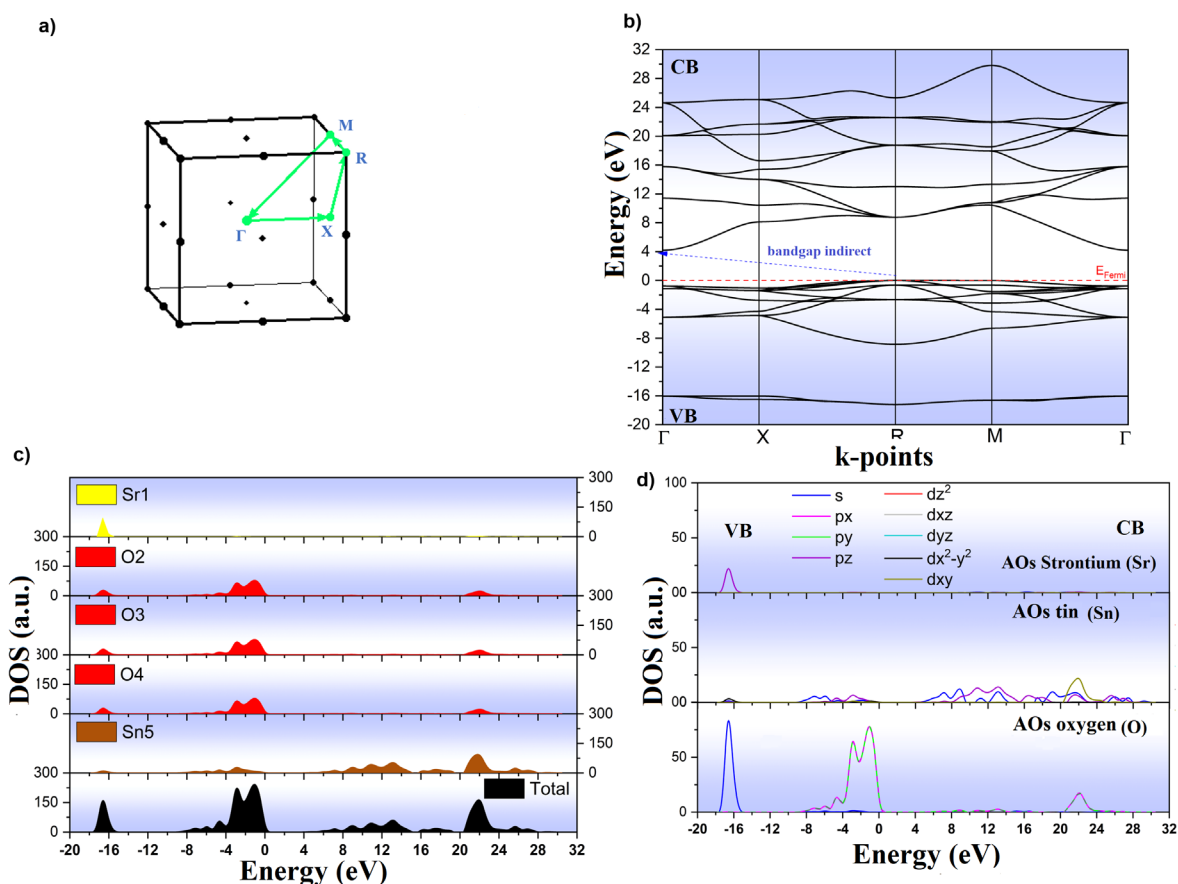
Fig. 3. (a) First Brillouin Zone path for cubic perovskites. Theoretical results of (b) Band Structure, (c-d) projection of total and partial DOS of the atoms, and atomic orbitals of the bulk $SrSnO_3$ perovskite structure.

In a second step, we investigate the distribution of the electronic density along the crystalline structure based on the charge density maps that graphically represent such results. In this analysis, isolines are used to represent the electronic density, and the understanding of these representations is a useful tool in the description of chemical bonds. In this case, we used the crystallographic plane in the direction (110) to analyze and locate the bonding interactions, as shown in Figure 4 (a-b).

Figure 4a represents the distribution of the electronic density for O, Sn, and Sr atoms that constitute the crystalline structure of $SrSnO_3$ forming two types of chemical bonds. First, the O-Sn-O interaction is characterized by a covalent interaction between these atoms, while the interaction between the O-Sr-O atoms is evidenced by ionic interaction. From the results of Figure 4b, it was possible to notice that the isolines are shared between the nuclei on the Sn-O bond axes, evidenced by the green color. Concerning the Sr and O atoms, the isolines are mostly concentrated on the nuclei, indicating the ionic character for the Sr-O interactions.
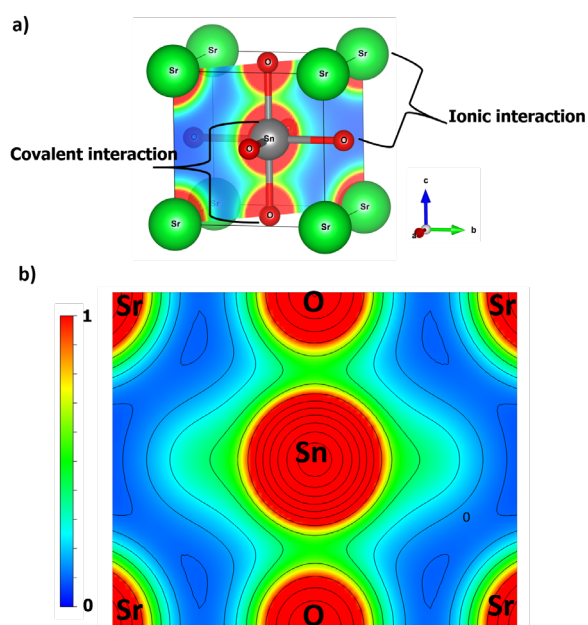
Fig. 4. (a-b) Results of the electronic density map in the diagonal plane (110) for the $SrSnO_3$ compound.

In addition to the charge map, another way to investigate the distribution of electron density around the nuclei is through the overlap between these densities that contributes to generating chemical bonds in the different clusters $[SrO_{12}]$ and $[SnO_6]$. For this purpose, Mulliken's Population Analysis [23] was employed. This methodology evaluates the distribution of electrons through the linear combination of atomic orbitals (LCAO), described by the basis set, to form molecular orbitals and the density matrix used to describe the electronic density behavior along with the crystalline structure.

In this framework, the positive signs indicate that the overlap is effective for the formation of the chemical bond, i.e., between the orbitals involved in the bond, there must be an effective overlap of the orbitals resulting in a constructive interaction of the wavefunctions, characterized by an accumulation of electronic density in the internuclear region, typically related to the covalent bonds. In contrast, the negative signs indicate that the overlap of the orbitals occurs through a destructive interaction disfavoring the formation of the chemical bond, resulting in an accumulation of the electronic density on the nuclei, typically associated with the ionic bond.

Based on the results related to population overlap for Sr-O and Sn-O bonds of bulk $SrSnO_3$ and the charge density map (Figure 4), it was possible to describe the formation of covalent bonds between the Sn and O atoms with a value of 0.154 and ionic interaction between the Sr and O with a value of -0.006.

3. Material and Methods

The calculations were performed using the CRYSTAL14 package within the framework of the density functional theory (DFT) and hybrid functional B3LYP [24-26] to calculate the structural parameters and perform the analysis of the electronic structure, following a series of theoretical studies for a wide variety of perovskite compounds [27, 34]. All-electron basis sets described the atomic centers according to

the CRYSTAL basis set library: 976-41(d51)G (s/sp/d), 9763111631 (s/sp/d) e 6-31G* (s/sp) for Sr, Sn and O, respectively. VESTA program was used to model the SrSnO3 structure and charge density maps.

The electronic integration was performed using a 4×4×4 Monkhorst-Pack [35] k-mesh containing 10 k-points for all models. The accuracy of the Coulomb and exchange integral calculations were controlled by five thresholds set to 8, 8, 8, 8, and 14. The converge criterion for mono- and bi-electronic integrals were set to 10^{-8} Ha. In contrast, the root-mean-square (RMS) gradient, RMS displacement, maximum gradient, and maximum displacement were set to 8×10^{-5}, 1.9×10^{-4}, 1.3×10^{-4}, and 3.8×10^{-4} a.u., respectively.

4. Conclusions

The simulations based on quantum mechanics and the experimental results allowed us to understand, interpret, and analyze the structural and electronic results at the atomic level. For the bulk, all the obtained results for the lattice parameters, bond distances, and bandgap were in agreement with the experimental results and other theoretical studies based on the Density Functional Theory.

Regarding the structural behavior, it was observed that the lattice parameters and the unit cell volume are associated with the cubic perovskite structure according to the XRD analysis. Concerning the analysis of electronic structure for $SrSnO_3$, it was possible to observe that, in general, the valence band is occupied by electronic states originating from O and Sr atoms, while Sn atoms occupy the conduction band. The bandgap was calculated as 4.18 eV, being an indirect electron transfer process. Moreover, the charge density map and the overlap analysis for the different $[SnO_6]$ and $[SrO_{12}]$ clusters confirm the covalent and ionic bond interaction, respectively.

Therefore, the theoretical results using the B3LYP functional combined with the basis set for Sr, Sn, and O, provided good results in the calculation of structural and electronic properties.

Acknowledgments

Author Contributions

Marta Maria de Moura Bezerra: Conceptualization of theoretical section, Investigation, Writing - original draft. Marisa Carvalho Oliveira: Conceptualization of theoretical section, Formal analysis, Investigation, Writing - review & editing, Visualization. Weber Duarte Mesquita: Conceptualization of theoretical section, Investigation, Writing - review & editing. Amilton Brito da Silva Junior: Writing - review & editing. Elson Longo: Writing - review & editing, Visualization, Funding acquisition. Maria Fernanda do Carmo

Gurgel: Writing - review & editing, Visualization, Supervision, Project administration.

References and Notes

[1] Shannon, R. D. *Acta Crystallogr. Sect, A: Found. Adv.* **1976**, *32*, 751. **[Crossref]**

[2] Liu, Y.; Zhou, Y.; Jia, D.; Zhao, J.; Wang, B.; Cui, Y.; Li, Q.; Liu, B. *J. Mater. Sci. Technol.* **2020**, *42*, 212. **[Crossref]**

[3] Zhong, F.; Zhuang, H.; Gu, Q.; Long, J. *RSC Adv.* **2016**, *6*, 42474. **[Crossref]**

[4] Montenegro, J. E.; Ochoa-Muñoz, Y.; Rodríguez-Páez, J. E. *Ceram. Int.* **2020**, *46*, 2016. **[Crossref]**

[5] Chen, Q.; Ma, S. Y.; Jiao, H. Y.; Zhang, G. H.; Chen, H.; Xu, X. L.; Yang, H. M.; Qiang, Z. *Ceram. Int.* **2017**, *43*, 1617. **[Crossref]**

[6] Kim, B. N.; Seo, G. K.; Hwang, S. W.; Yu, H.; Ahn, B.; Seo, H.; Cho, I. S. *Ceram. Int.* **2018**, *44*, 1843. **[Crossref]**

[7] Gómez-Solís, C.; Oliva, J.; Diaz-Torres, L. A.; Bernal-Alvarado, J.; Reyes-Zamudio, V.; Abidov, A.; Torres-Martinez, L. M. *J. Photochem. Photobiol., A* **2019**, *371*, 365. **[Crossref]**

[8] Teixeira, A. R. F. A.; de Meireles Neris, A.; Longo, E.; de Carvalho Filho, J. R.; Hakki, A.; Macphee, D.; dos Santos, I. M. G. *J. Photochem. Photobiol., A* **2019**, *369*, 181. **[Crossref]**

[9] Zhang, X.; Hu, J.; Cao, Y.; Xie, J.; Jia, W.; Wang, S.; Jia, D. *Chem. - Eur. J.* **2018**, *24*, 14111. **[Crossref]**

[10] Zhang, Y.; Wang, J.; Sahoo, M. P. K.; Shimada, T.; Kitamura, T. *Phys. Chem. Chem. Phys.* **2017**, *19*, 26047. **[Crossref]**

[11] Mountstevens, E. H.; Attfield, J. P.; Redfern, S. A. T. *J. Phys.: Condens. Matter.* **2003**, *15*, 8315. **[Crossref]**

[12] Glerup, M.; Knight, K. S.; Poulsen, F. W. *Mater. Res. Bull.* **2005**, *40*, 507. **[Crossref]**

[13] Glazer, A. *Acta Crystallogr., Sect. B: Struct. Sci., Cryst. Eng. Mater.* **1972**, *28*, 3384. **[Crossref]**

[14] Gao, Q.; Li, K.; Zhao, L.; Lv, K.; Li, H.; Zhang, J.; Du, W.; Liu, Q. *J. Mater. Chem. C.* **2020**, *8*, 3545. **[Crossref]**

[15] Megaw, H.D. *Proc. Phys. Soc.* **1946**, *58*, 133. **[Crossref]**

[16] Alves, M. C. F.; Marinho, R. M. M.; Casali, G. P.; Siu-Li, M.; Députier, S.; Guilloux-Viry, M.; Souza, A. G.; Longo, E.; Weber, I. T.; Santos, I. M. G.; Bouquet, V. *J. Solid State Chem.* **2013**, *199*, 34. **[Crossref]**

[17] Cho, H.J.; Sato, K.; Wei, M.; Kim, G.; Ohta, H. *J. Appl. Phys.* **2020**, *127*, 115701. **[Crossref]**

[18] Cassia-Santos, M. R.; Mendes, S. B.; Gurgel, M. F. C.; Figueiredo, A. T.; Godinho Jr., M.; Braz, C. E. M.; Longo, E. *Cerâmica* **2014**, *60*, 259. **[Crossref]**

[19] Vegas, A.; Vallet-Regi, M.; Gonzalez-Calbet, J. M.; Alario-Franco, M. A. *Acta Crystallogr., Sect. B: Struct. Sci., Cryst. Eng. Mater.* **1986**, *42*, 167. **[Crossref]**

[20] Liu, Q.; Dai, J.; Zhang, X.; Zhu, G.; Liu, Z.; Ding, G. *Thin Solid Films* **2011**, *519*, 6059. **[Crossref]**

[21] Weston, L.; Bjaalie, L.; Krishnaswamy, K.; Van de Walle, C.G. *Phys. Rev. B.* **2018**, 97, 054112. **[Crossref]**

[22] Bannikov, V. V.; Shein, I. R.; Kozhevnikov, V. L.; Ivanovskii, A. L. *J. Magn. Magn. Mater.* **2008**, *320*, 936. **[Crossref]**

[23] Mulliken, R. S. *J. Chem. Phys.* **1955**, *23*, 1833. **[Crossref]**

[24] Dovesi, R.; Orlando, R.; Erba, A.; Zicovich-Wilson, C. M.; Civalleri, B.; Casassa, S.; Maschio, L.; Ferrabone, M.; De La Pierre, M.; D'Arco, P.; Noël, Y.; Causà, M.; Rérat, M.; Kirtman, B. *Int. J. Quantum Chem.* **2014**, *114*, 1287. **[Crossref]**

[25] Lee, C.; Yang, W.; Parr, R. G. *Phys. Rev. B: Condens. Matter Mater. Phys.* **1988**, *37*, 785. **[Crossref]**

[26] Becke, A. D. *J. Chem. Phys.* **1988**, *88*, 1053. **[Crossref]**

[27] Longo, V. M.; de Figueiredo, A. T.; de Lázaro, S.; Gurgel, M. F.; Costa, M. G. S.; Paiva-Santos, C. O.; Varela, J. A.; Longo, E.; Mastelaro, V. R.; Vicente, F. S. D.; Hernandes, A. C.; Franco, R. W. A. *J. Appl. Phys.* **2008**, *104*, 023515. **[Crossref]**

[28] Longo, V. M.; Cavalcante, L. S.; Costa, M. G. S.; Moreira, M.L.; de Figueiredo, A. T.; Andrés, J.; Varela, J. A.; Longo, E. *Theor. Chem. Acc.* **2009**, *124*, 385. **[Crossref]**

[29] Maul, J.; Santos, I. M. G.; Sambrano, J. R.; Erba, A. *Theor. Chem. Acc.* **2016**, *135*, 36. **[Crossref]**

[30] Maul, J.; Erba, A.; Santos, I. M. G.; Sambrano, J. R.; Dovesi, R. *J. Chem. Phys.* **2015**, *142*, 014505. **[Crossref]**

[31] Moreira, M. L.; Longo, V. M.; Avansi, W.; Ferrer, M. M.; Andrés, J.; Mastelaro, V. R.; Varela, J. A.; Longo, É. *J. Phys. Chem. C.* **2012**, *116*, 24792. **[Crossref]**

[32] Longo, V. M.; Cavalcante, L. S.; Erlo, R.; Mastelaro, V. R.; de Figueiredo, A. T.; Sambrano, J. R.; de Lázaro, S. Freitas, A. Z.; Gomes, L.; Vieira, N. D.; Varela, J. A.; Longo, E. *Acta Mater.* **2008**, *56*, 2191. **[Crossref]**

[33] Desmarais, J. K.; Erba, A.; Dovesi, R. *Theor. Chem. Acc.* **2018**, *137*, 28. **[Crossref]**

[34] Mesquita, W. D.; de Cassia-Santos, M. R.; Espinosa, J. W. M.; Leal, S. H. B. de S.; Longo, E.; Gurgel, M. F. C. *Orbital: Electron. J. Chem.* **2019**, *11*, 91. **[Crossref]**

[35] Monkhorst, H. J.; Pack, J. D. *Phys. Rev. B: Condens. Matter Mater. Phys.* **1976**, *13*, 5188. **[Crossref]**

How to cite this article